An Unobtrusive Method for Remote Quantification of Parkinson's and Essential Tremor using mm-Wave Sensing

An Unobtrusive Method for Remote Quantification of Parkinson's and Essential Tremor using mm-Wave Sensing

Nazia Gillani, *Graduate Student Member*, *IEEE*, Tughrul Arslan, *Senior Member, IEEE,* and Gillian Mead

***Abstract*—Tremor is a primary symptom of common movement disorders such as Essential tremor and Parkinson's disease. People experiencing tremors face difficulty in performing everyday tasks which negatively impacts their independence. Tremor quantification helps clinicians in evaluating disease progression and treatment response. Majority of the existing methods include cameras or motion sensors embedded in wearables and hand-held devices. The continuous wearing of contact sensors can be uneasy for the patients while the cameras cause privacy concerns. This paper proposes a novel method for tremor quantification using a Frequency Modulated Continuous Wave (FMCW) radar sensor. In this paper, an off-the shelf, low-cost FMCW radar has been configured to capture vibrations induced in distal limbs, a representative feature of Essential and Parkinson's Tremors. Moreover, a signal processing chain is developed to extract characteristic tremor frequency and amplitude by reconstructing the tremor signal from the radar return signals. For robustness and increased accuracy, static clutter and voluntary body motion are eliminated. Extensive experiments were performed and results were compared to the state-of-the-art methods that use accelerometers and gyroscopes. A strong correlation (R^2>0.97) is found between the reference sensor readings and predicted values for both quantified parameters. The mean error for the frequency and amplitude is 0.14Hz and 0.03cm, respectively. Results demonstrate a superior accuracy as compared to the existing non-contact techniques, with the added advantage of privacy and integrity preserving for the end-user. Hence, the proposed system can provide reliable long-term objective assessment, aiding clinicians in the evaluation of tremor severity and treatment effectiveness.**

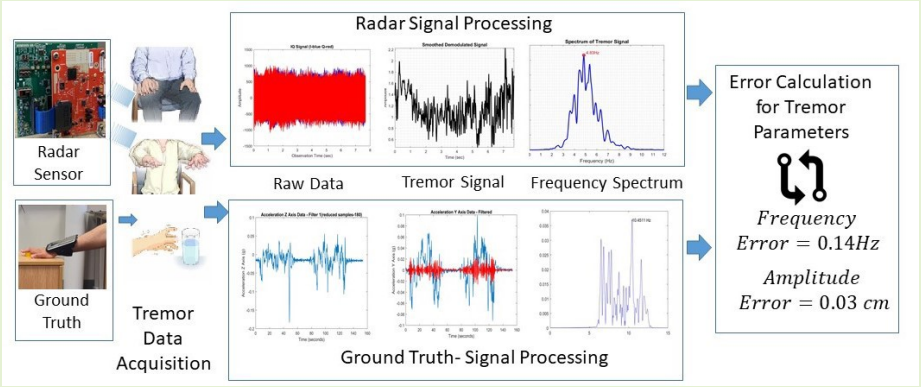

***Index Terms*— Tremor quantification, FMCW radar, Healthcare, Parkinson's disease, Essential tremor, Movement Disorders, Signal Processing, Remote monitoring, Non-contact sensing, Independent Living**

I. Introduction

TREMOR is a motor disorder in which unintentional and uncontrollable oscillations are experienced in certain parts of the body especially in the distal limbs [1],[2]. Globally, millions of people are affected by tremors. People suffering from tremors experience difficulty in performing simple yet essential everyday activities such as eating, drinking or arm extension to grasp something. Consequently, tremors not only negatively affect the Quality of Life (QoL) and independence but also increase fall risk in patients who have low cognition [3], [4]. Tremor is a characteristic feature of progressive neurological diseases, such as Essential Tremor (ET) and Parkinson's disease (PD). ET is one of the most widely spread movement disorders worldwide [5]. For people aged between 40 and 60 years, the incidence rate is 4-5%. This increases to 9% for people aged 60 years or more [6]. Whereas, the statistics report of 2019 shows that more than 8.5 million individuals suffer from PD causing 5.8 million disability-adjusted life years [7]. This marks an alarming increase of 81% since the year 2000 [7]. Parkinsonian tremors and other hyperkinetic conditions may also occur as a later manifestation in stroke patients [8]. With such high incidence rates, and keeping in view the fact, that these neurological diseases cannot be cured, effective and feasible methods are required for the continuous quantification of these patients living independently.

Disease progression and treatment heavily rely on the quantification of key tremor characteristics. Clinically, tremor severity is assessed using qualitative rating scales such as Quality of Life in Essential Tremor (QUEST) [9], Essential Tremor Rating Scale (ETRS) [10] and Unified Parkinson's Disease rating Scale (UPDRS) [11]. Though these clinical tests indicate the disease severity, however, they are time-consuming, subjective and sporadic, which may cause a hindrance in portraying accurate picture of disease progression

[12]. Continuous monitoring can lead to an early diagnosis of further neurological deterioration, assessment of disease progression and help the clinicians in evaluating treatment effectiveness [13]. Tremor frequency and amplitude are two clinically significant parameters that indicate tremor severity[14]–[17]. Both parameters are vital in the differential diagnosis of tremor-related diseases, for example, to rule out PD versus ET, where symptoms might be confusing [18]. Table 1 demonstrates the characteristic fundamental frequency of PD and ET [19], [20]. However, the amplitude of the tremor depends on multiple factors including age, type of tremor and the time elapsed since the onset of the disease. In the literature, the typical tremor amplitude ranges have been reported to be between 0.1 cm for mild tremors going up to 4 cm for severe tremors [21], [22].

TABLE I
CHARACTERISTIC FUNDAMENTAL TREMOR FREQUENCY

Aetiology	Rest Tremor	Action Tremors	
		Postural	*Kinetic*
PD	4-6 Hz	6-8 Hz	-
ET	-	5-8 Hz	5-12Hz

II. RELATED WORK

Various sensors are used for the quantification of tremor parameters. The sensors measure the limb vibrations induced as a result of tremors. This section details the various sensors and methods that exist in the literature that have been used to quantify tremors.

A. Tremor Quantification through Wearables

Conventional Electroencephalography (EEG) and Electromyography (EMG) techniques are used to monitor signals from the central nervous system and muscles for detecting tremor motor dysfunction [23]–[25]. Recently, wearable motion sensors such as accelerometers and gyroscopes are widely being adopted for the said purpose. These sensors are either used as stand-alone units worn on the upper and lower limbs [26]–[29] or are the ones embedded in daily-use devices such as smartwatches and smartphones [30]–[33]. Algorithms are developed to process the raw data collected from the accelerometer and gyroscope axes. The fundamental frequency is calculated by performing the power spectral density analysis. Whereas, the amplitude is calculated by either performing a single integration on the gyroscope data or a double integration on the accelerometer readings [24]-[34]. A gyration computer mouse has also been used to track the stability in drawing tasks to quantify tremors [35]. For the EEG and EMG recordings, specialized lab equipment is required, while the continuous wearing of the contact sensors can result in the patient being uncomfortable. Moreover, patients also suffering from cognitive issues may altogether forget to wear them. Handheld devices such as smartphones or the computer mouse can't be held for too long. Hence these techniques result in missing tremor episodes throughout the day, hindering the continuous objective monitoring of tremors.

B. Tremor Quantification through Camera Sensors

In the literature, a handful of non-contact solutions also exist. A recent systematic review [36], cites multiple works that use camera-based sensors for the quantification of hand tremors. Similarly, [37] and [38] have used Kinect technology using colour and depth cameras for detecting and quantifying tremors. However, the continuous use of cameras and video recording invades the privacy of an individual. Moreover cameras are light dependent. Hence, non-contact and privacy preserving solutions are required for long-term reliable tremor quantification.

C. Tremor Quantification using Electromagnetic Sensors

Recently electromagnetic (EM) sensors have gained popularity in numerous healthcare applications. This is due to their ability to monitor relevant parameters that are indicative of health status of an individual such as heartrate detection and gait monitoring [39], [40]. Wi-Fi and radar sensors both fall in this category. Though EM sensors have been used for a variety of healthcare applications, their evaluation for tremor quantification due to ET and PD, specific to care-based scenarios is non-existent. For example, out of the existing studies in the literature, [41] and [45] have quantified tremors, whereas [43] and [44] only detect action tremors during drinking water. Blumrosen et al. [41] used an Ultra Wideband (UWB) radar system to quantify tremor frequency and amplitude. The radar system is based on discrete components and hence is large in size. Moreover, discrete components increase overall system cost and power consumption [42]. A Linear Minimum Mean Square Error criteria was used with matched filtering. Though the system quantified frequency with sensible accuracy however, for the tremor amplitude, the accuracy declined with increasing distance from 1m to 1.5 m and 2m of the robotic arm from the radar system. In [43], the change in variance of the subcarrier amplitude from an S-band wireless router and a receiving omnidirectional antenna is used to distinguish between tremor and no tremor episodes while a person grabs a glass of water. In [44], an FMCW radar has been used to detect action tremors employing time-frequency analysis. In [43] and [44] though tremor has been identified, however, the tremor parameters have not been quantified. More recently, a 2x2 array 10 GHz X band Doppler radar sensor was developed to quantify hand tremors. [45]. Tremor quantification is done for digital hand-writing scenarios for PD patients. The system correlated ($R^2 > 0.85$) three time-domain parameters: zero crossing, Willison amplitude and waveform length to the tremor frequency. The measurement resolution of the system is 20-40 cm. Hence, the system is limited to quantifying hand tremors at very small range and is not suitable for continuous monitoring in independent living scenarios. The performance evaluation of the proposed system has been done against an Apple pencil, laptop and smartphone.

Keeping in view the limitations of the current studies, the aim of this paper is to quantify tremors for general care-based scenarios that encompass all the major activities that can trigger tremors throughout the day. This has been done keeping in view the needs of the elderly population who suffer from tremors due to neurological dysfunction such as Essential Tremor (ET) and Parkinson's disease (PD). The main objective of this research

is to demonstrate the effectiveness, feasibility and accuracy of an FMCW radar system to quantify tremor parameters for use cases of independent care while preserving the privacy and integrity of the patient. In contrast to the existing techniques which have been developed to account for hand tremors only, the proposed system is a more general purpose specifically tailored and designed to quantify Essential and Parkinson's tremors in real-life like settings.

The system has been designed to account for tremors that occur throughout the day while performing certain actions or while sitting relaxed in a chair. . These include actions such as eating or drinking (action tremors), a front extension of the upper limbs to hold it against gravity (posture tremor) and while the patient is relaxing such as sitting in the chair (rest tremors). Action and posture tremors are characteristic of ET while rest tremors are a key symptom in PD patients. In summary, the key contributions of this work are as follows:

1) This paper presents a novel system that quantifies tremors specific to ET and PD patients for general care based scenarios with focus on independent living.
2) The chirp parameters of a commercial off-the-shelf CMOS FMCW radar on-chip sensor system, have been designed to tailor the sensor specifically to capture tremors in the distil limbs. The single chip reduces the overall cost and power of the system unlike the discrete component systems used in [41] and [43]. The system is easily portable making it suitable for deployment for continuous remote monitoring of tremor patients in the ease of their homes while preserving their privacy and integrity.
3) An algorithm was developed to quantify two clinically important tremor parameters, frequency and amplitude. In contrast to the existing studies that quantify tremors using time series data or numerical analysis techniques using radar this algorithm is implements a mathematical vibrational model and utilizes phase preservation from the radar return signals.
4) Extensive experiments were performed for action, posture and rest tremors. Results were validated through state-of-the-art conventional methods that use accelerometer and gyroscope data [25]-[33]. A detailed statistical analysis is performed on the obtained results. The overall signed-errors ± SD for the predicted frequency and amplitude are -0.14 ± 0.4 Hz and -0.03 ± 0.1 cm respectively. The results demonstrate a superior accuracy as compared to existing unobtrusive methods to accurately quantify tremors.

For validation purposes, the accelerometer and gyroscope sensors embedded in the iPhone were used as a reference. The data from these sensors were obtained using a mobile application 'TREMOR12' [46]. The choice of this application as a validation tool is based on the following factors:

a) The mobile application is compatible with the current regulatory oversight by the European Union (MEDDEV) guidance and the Food and Drug Administration (FDA) for medical mobile applications [46].
b) The application has been tested and evaluated on ET patients aged 55-71 years [47].
c) The application developer and the first author of [46], is a neurosurgeon and experienced mobile application developer. The co-authors are also associated with the departments of Neurology, Psychiatry, and Neurosurgery at the Medical centre of Maastricht University, Netherlands.

The subsequent sections of the paper are: Section III describes the data acquisition system used for tremor quantification. Section IV details the signal processing chain developed to extract tremor frequency and amplitude from the raw radar data. Section V presents the experimental protocol and detailed results.

III. Hardware System

This section discusses the motivation behind the use of the FMCW radar and presents the details of the data acquisition hardware. Then the customized configuration applied to the radar sensor to detect tremors are presented.

A. Motivation for millimetre Wave FMCW Radar

Radar sensors are excellent electromagnetic (EM) sensors whose performance is not affected by the atmosphere, clothing of the patient and light conditions of the room. The radar used in this work is a millimetre Wave (mmWave) sensor, with a wavelength in the mm range. This gives an advantage of the small size of transmitting (Tx) and receiving (Rx) antennas and hence, a compact form factor for the sensor, facilitating portability, a desired aspect for remote health monitoring. The advent of the new generation of low-cost, compact-size mmWave sensors has paved the way for various medical, military and industrial applications[48], [49],[50]. FMCW radars are continuous wave radars that transmit the signal continuously as compared to the periodic pulses in pulse radars. This improves the signal-to-noise ratio (SNR) [51]. Moreover, unlike the simple Continuous Wave (CW) radar, the FMCW transmits a frequency-modulated signal with finite bandwidth (BW). This facilitates clutter isolation and aids in velocity and range measurements of the target in front of the radar [52]. With specialized algorithms, these properties can be used to keep track of the subtle changes in the range of the object thus making the FMCW radar a suitable choice for Tremor quantification.

B. Data Acquisition System

Traditional radar systems have discrete components such as antennas, analogue components e.g. the clock, microcontrollers, Analog-to-Digital (ADC) converters and Digital signal processors (DSP) [52]. However, using these discrete components gives rise to increased energy losses, increased power consumption and larger system space requirement [42]. The sensor used in the current study is a 77 GHz CMOS-based, linear FMCW radar system on a chip manufactured by Texas Instruments [53]. All the components are integrated on a single chip mitigating the above-mentioned issues. It has a programmable C674x DSP core and an ARM Cortex®-R4F Microcontroller [54]. The board is powered by a 5V adapter. The sensor is provided with real and quadrature mixers. Depending on the target application, the sensor can be programmed to select any mixer. The output of the mixers

results in continuous beat signals also known as Intermediate Frequency (IF), as shown in figure 1.

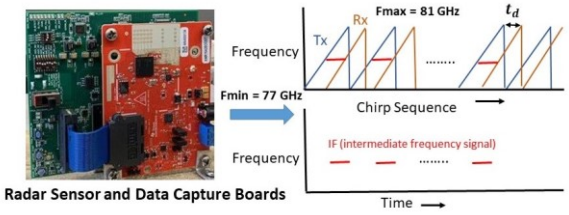

Fig. 1. FMCW Radar System and IF Signal Generation

The IF signals are then digitized by the Analog-to-Digital (ADC) converters. To capture these sampled IF signals a TI data capture board DCA1000 is used [55]. The data is transferred to the DCA1000 through the 60-pin Samtec cable also shown in figure 1. These are then sent to the computer via an Ethernet connection.

C. Customizing the Radar sensor for Tremor Detection

As FMCW radars are used for a variety of sensing applications, the system requirements vary depending on the targeted objective. A sensor configured for autonomous driving assistance will vary as compared to medical sensing application. The sensor has to be programmed according to the range requirements, environmental conditions (indoor versus outdoor) and the desired field of view (FOV). In this work, the radar sensor system was configured for indoor requirements which could detect and monitor small tremor vibrations.

The radar system used provides flexibility in configuring chirp timing parameters. This is done by using the mmWave Studio® [56]. Using the mmWave Studio IDE, the digital timing engine, local oscillator, ADC sampler and processor are programmed to control the chirp start time 'T_s', idle time (time taken to restart the synthesizer for the new chirp), chirp slope 'S' and chirp end time as shown in figure 2.

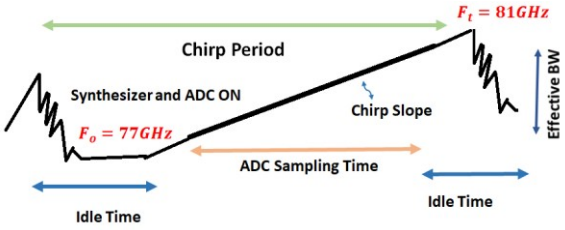

Fig. 2. Programmable FMCW Chirp

Suppose an object is at a distance 'd' from the radar, then the reflected signal is delayed by a time 't_d' with respect to the transmitted signal, as indicated in figure 1. The time delay is given as t_d =2d/c, where 'c' represents the speed of light and 2 accounts for the round trip in the case of the collocated radar. The instantaneous phase φ_{IF} and frequency f_{IF} of the IF signal are given by the differences in the corresponding instantaneous values of the transmitted and received signals. The phase is given as

$$\varphi_{IF} = 2\pi f_{IF} t_d \quad (1)$$

Inserting the value of $'t_d'$ in (1) gives:

$$\varphi_{IF} = 4\pi d/\lambda \quad (2)$$

From (2), it is seen that a small variation in 'd' results in a corresponding phase change. This can be leveraged to approximate the range of the target. To resolve the range values, the Fast Fourier transform (FFT) is applied to the sampled signals, also called range-FFT. According to FFT theory, the frequency resolution increases if the length of the IF signal is increased [49]. The phase of the range FFT calculated from the reflected signal changes completely by 180 degrees for every 1 mm of range change [50]. This property is crucial for estimating vibration frequencies and algorithms are required for accurate phase unwrapping [58]. From figures 1 and 2 it can be seen that a larger BW will result in a longer IF signal. The property of the radar to distinguish between two near objects is known as Range resolution 'R_{res}' and is given by:

$$R_{res} = c/2BW \quad (3)$$

The range resolution for the radar used is 3.74 cm. Hence, two distinct vibrating objects such as dominant and non-dominant limbs can easily be distinguished. Tremors experienced in the limbs can be irregular or regular depending on the underlying neurological conditions. For example, in a resting tremor, the amplitude may vary over time making it irregular. This affects the velocity of the limb. To measure the velocity changes, a series of equally spaced chirps are transmitted. To monitor the changing velocity 'v', the chirp time 'T_{ch}' should be controlled. The chirp time and phase change are related by:

$$\Delta\varphi_{IF} = 4\pi v T_{ch}/\lambda \quad (4)$$

From figure 2, it can be observed that $'T_{ch}'$ depends on the slope of the chirp 'S' and BW. However, the synthesizer takes some time to synthesize every new chirp. This time is known as idle time. This limits the overall T_{ch} and the effective BW of the sensor. The measurable maximum velocity increases with the frame time $'T_{Frame}'$ that is, a greater number of chirps per frame. Whereas, the velocity resolution increases with a shorter chirp period also known as fast FMCW [59]. For applications where the frequency is very low such as breathing detection (0.1 – 0.5 Hz), a low number of chirps per frame is enough to guarantee that no phase rollover occurs. However, a fast chirp period along with a higher number of chirps per second is required for applications such as heart rate variability [52].

In this work, T_{ch} (=BW/S) was programmed to be 0.3 msec, which means 3333.3 chirps per second are transmitted. This ensures the detection of frequency vibrations for tremors (4-12 Hz). Table II summarizes the designed parameters and their values used in this work.

TABLE II
PROGRAMMED CHIRP PARAMETERS

Parameter	*Symbol*	*Value*	*Units*
Bandwidth used	BW	3.60	GHz
Sampling rate	-	5	MSps
Samples per chirp	N	256	-

Parameter	*Symbol*	*Value*	*Units*
Frames	nF	200	-
Chirps in one Frame	-	128	-
Chirp Time	T_{ch}	0.3	ms
Frame periodicity	p	40	ms
Range Resolution	R_{res}	4	cm
Field of View	FOV	120	degrees
Max. detectable Range	Rmax	9.4	m
Data Capture Time	T_{Total}	8	sec

IV. Signal Processing Chain

This section explains the signal conditioning and pre-processing steps for the received signal. It discusses the FMCW signal model for tremor vibrations and finally details the algorithm developed to extract tremor frequency and amplitude.

A. Signal Pre-processing

The relative length of the vibrating limb is considerably smaller as compared to the full body thus affecting the radar cross section (RCS). The reflections from the vibrating limbs are weak as compared to the strong interference signals from the surroundings and bulk body movements. These strong reflections are superimposed on the weak vibrating modulated signal. This problem gets pronounced when the vibration frequency f_v is also low [49], as in the case of Parkinson's disease rest tremors.

An important consideration is the use of real (I only) versus quadrature (I and Q) mixtures. The TI radar sensor allows using either [57]. For this work, the sensor was programmed to use a quadrature mixer with complex baseband (BB) architecture. The received input is mixed with sin and cos versions of the transmitted signal. Real BB signals from real mixers result in a double sideband (DSB) signal whereas, complex BB signals from quadrature mixers give a single sideband (SSB) spectrum [55]. The DSB and SSB receiver signals are given as:

$$Rx_{DSB} = \cos[(\tfrac{4\pi}{\lambda})D_v(t) + (\tfrac{4\pi}{\lambda})R_0]\cos(2\pi f_{IF}t) \quad (5)$$

$$Rx_{SSB} = \cos[2\pi f_{IF}t + (\tfrac{4\pi}{\lambda})D_v(t) + (\tfrac{4\pi}{\lambda})R_0] \quad (6)$$

From (5) it can be seen that at a range $'R_0'$ from the radar, the received signal is the sine wave function with frequency f_{IF}, with an envelope modulated by limb tremor vibration function $D_v(t) = D_{max}\sin(2\pi f_v t)$. This is illustrated in figure 4. Hence, the IF signal spectrum suffers image band noise foldback, reducing the SNR. In comparison, the tremor vibration in SSB (6), is embedded in the phase part of the received input signal. This, unlike the DSB, eliminates the problem of null points and optimum points. Moreover, in SSB the in-band (where the signal of interest lies) and image-band remain distinguished thus increasing performance gain up to 3 dB in noise figure [57]. For these reasons, the radar sensor was programmed to use a quadrature mixer and complex baseband architecture, resulting in SSB received signal.

B. FMCW Signal Model for Vibrating Limb

The transmitted FMCW chirp for a single period 'T_{ch}' is:

$$Tx(t) = A_T\exp(j(2\pi f_0 t + \pi S t^2 + \varphi)) \quad (7)$$

Where $'\varphi'$ denotes the initial phase, f_0 is the start frequency of the chirp, A_T is the transmit power amplitude, $'S'$ indicates the chirp slope and 't' denotes the fast time within one time period 'T_{ch}'.

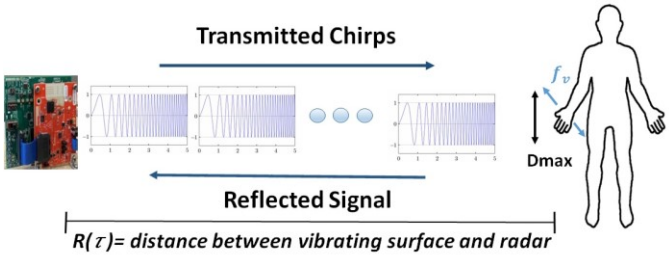

Fig. 3. Modeling Radar Return Signal from Vibrating Limb

$'R_0'$ is the distance of the subject from the radar system and $R(\tau)$ is the time-varying range which incorporates the varying range from the vibrating limbs due to tremors. $R(\tau)$ of the vibrating limb from the radar at any given time will be:

$$R(\tau) = R_0 + D_v(t) \quad (8)$$
$$R(\tau) = R_0 + D_{max}\sin(2\pi f_v t) \quad (9)$$

D_{max} is the maximum vibrational amplitude. The typical maximum value for rest tremors is 2cm while for action tremors this can increase to 3 or 4 cm [20], [21]. τ is the slow radar time and depends on the total chirps transmitted. The signal that is reflected from the subject is a delayed version of the transmitted signal. Hence, the received signal for a single chirp is

$$Rx(t) = Tx(t) - Tx^*(t - t_d)) \quad (10)$$
$$Rx(t) = A * \exp(j(2\pi f_0 t_d + 2\pi S t_d t - \pi S t_d^2)) \quad (11)$$

'A' is the amplitude of the signal. This is dependent on the RCS and propagation attenuation. The third term in (11) can be ignored because the slope is of the order MHz/s while due to the programmed fast FMCW chirps, the t_d is in nanoseconds. For slow-moving targets, such as human motion, the range can be considered constant within one time period [58]. This assumption cannot be applied to high-speed targets such as the rotor blades of a quadcopter or helicopter [59]. Mathematically, the change in range in one time period 'T_{ch}', should be less than $c/2f_c$ [60]. In this case, this approximately comes out to be 1.95 mm within 0.3ms, hence, meeting the condition. Thus, the received signal can be approximated as:

$$Rx(t) = A*\exp(j(2\pi f_0 t_d + 2\pi S t_d t)) \quad (12)$$

Inserting the value of t_d in (12), the beat frequency f_b and the standard slow time phase history come out to be:

$$f_b = 4\pi\frac{R(\tau)}{\lambda} \text{ and } \varphi_{IF}(t) = 4\pi S R_0/c \quad (13)$$

Hence, for accurate extraction of the slow time range profile, phase preservation is the key [59].

C. Signal Processing

After collecting the raw radar data, the signal processing was performed in MATLAB R2022a. The complex ADC sampled signals from the radar are obtained in .bin format. These were converted to .mat files using a MATLAB snippet. This resulted in a column vector. The size of the data vector is dependent on the total number of frames, ADC samples and the total number of chirps transmitted. From table 2, it can be seen that the size of the column vector turns out to be 6553600x1. The column vector is then reshaped into a fast versus slow time matrix with a size of 256x25600. Each column represents distinct chirps (fast time) while all the transmitted chirps are stacked together such that the rows represent the slow time. The Fast Fourier Transform (FFT) is performed on each chirp giving the range profile matrix. Static clutter was removed using a low pass filter, eliminating high-frequency reflections from the surroundings. To identify the target, range gating was performed. This was done by selecting the range bin with maximum amplitude after comparison along the successive range bins. At this stage, the DC offset was also removed for constellation correction as done in [61]. The random body motion was cancelled out based on signal energy as the voluntary body movements are not oscillatory and have a comparatively larger amplitude [62]. Hence, the signal was divided into small time frames of one second each. The energy for each time segment was calculated and if the calculated energy was greater than a certain threshold the samples in the segment were discarded. From the identified range bin, a 1-D tremor signal is synthesized by selecting the optimal range bin and summing the absolute of the selected range bin. Arctangent demodulation for phase unwrapping was performed. The demodulated signal was smoothed and passed through a 3rd order Butterworth band-pass filter. The centre frequency is set to 8 Hz while the bandwidth is 4 Hz. This has been chosen per the tremor frequency range of 4 Hz to 12 Hz. Finally, the spectral analysis of the tremor signal is performed by applying zero padding and using a hamming window and performing FFT. The maximum frequency is extracted which denotes the tremor fundamental frequency. Finally, the tremor amplitude is calculated by using (8) and (9) D_{max} for the rest tremors were taken as 2cm while for action and posture tremors it was taken as 4cm, per the existing literature [21], [22]. A flow diagram showing the radar signal processing is given in figure 4 below.

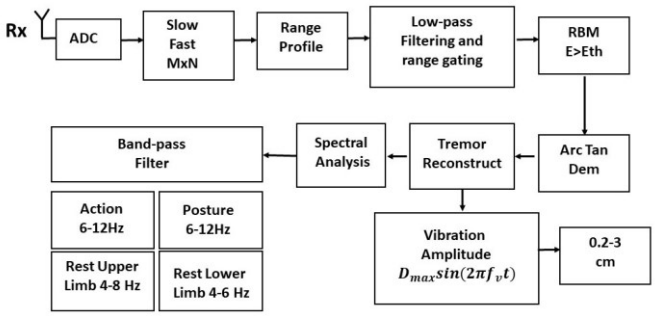

Fig. 4. Radar Signal Processing Flow Chart

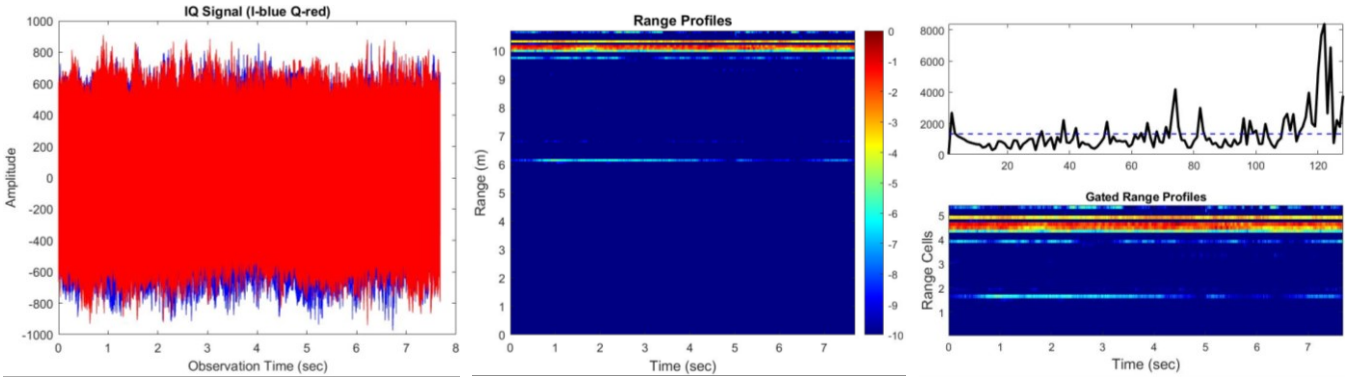

(a) (b) (c)

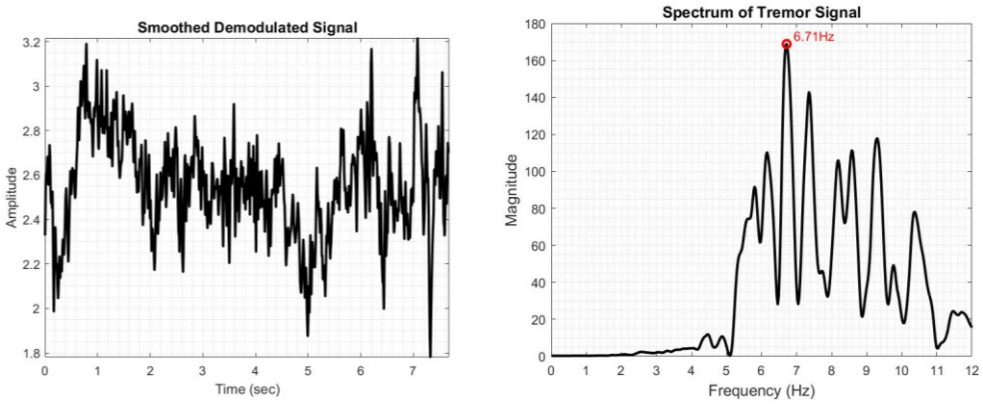

(d) (e)

Fig. 5. Radar Signal Processing for Action Tremor Trial (a) raw data (b) Range Profile (c) Range Bin Selection (d) 1-D Tremor Signal (e) Tremor Frequency

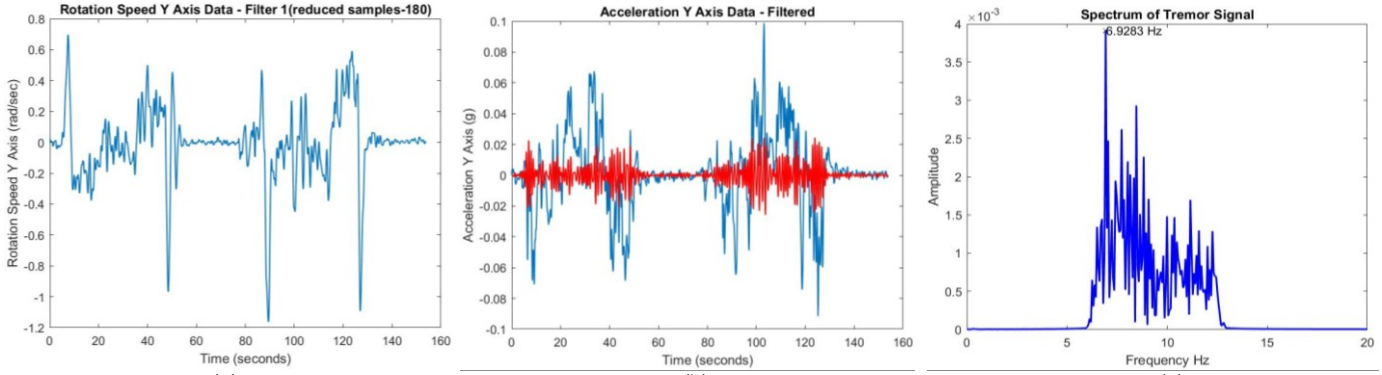

(a) (b) (c)

Fig. 6. Tremor12 Mobile Application Signal Processing for Action Tremor Trial (a) Raw Gyroscope Data (b) Noise Filtering (c) Tremor Frequency

V. Experimental Validation and Results

Tremors are majorly classified as either resting tremors, which occur while the muscles are relaxed or action tremors. Action tremors are further classified as kinetic and postural tremors [63]. Kinetic tremors occur when an individual performs voluntary tasks such as eating and posture tremors can get triggered when patients extend their arms and hold them in a position against gravity. ET and PD, though both are neurological diseases that cause tremors, however, their presentations are noticeably different. Action tremor is more associated with ET while rest tremor is one of the earliest signs in PD patients [64]. However, as the diseases progress, ET patients might develop rest tremors. While, in the case of PD, as the disease progresses motor dysfunction worsens thus patients experience action tremors as well [18].

A total of 60 experiments were conducted for various tremors. Activities were performed that induce action, postural and rest tremors. For each kind of tremor quantification, a total of 15 experiments were performed. Out of these 15 experiments, five involved no tremor trials and 10 experiments involved tremor-induced experiments. Each experiment lasted about 8 seconds. For true comparison between the proposed methodology and the base sensor random movements were excluded that arose when the button for the mobile application is pressed to start and stop data capture for the mobile application. Hence, a longer reading was taken for the mobile application. The table below details the list of experiments performed for data collection.

TABLE III
Experiment Details

Tremor Type	Without Tremor Trials	With tremors Induced Trials	
		Dominant Limb	Non-Dominant Limb
Action	5	10	-
Postural	5	5	5
Rest (Upper limbs)	5	5	5
Rest (Lower limbs)	5	5	5
Sub-Total	**20**	**25**	**15**
Total			***60***

For this proof of concept study, the subjects involved are healthy. They were advised to simulate tremors. The study was approved by the university's School of Engineering ethical review board. Data was collected simultaneously from the radar sensor, placed at position A and iPhone, placed at position B, as shown in figure 7. The mobile was securely attached to the distal limbs of the subject using a mobile holder as shown in figure 7. The radar is programmed for near-field application which allows a maximum of 9.4 m range detection. However, keeping in view the average room dimensions in homes, the subject was asked to sit at a distance of more than 3 m and less than 9 m from the sensor. From figure 5 (b) the range of the

subject can be observed to be slightly greater than 6 m. A varying distance was advised to check the robustness of the tremor quantification system.

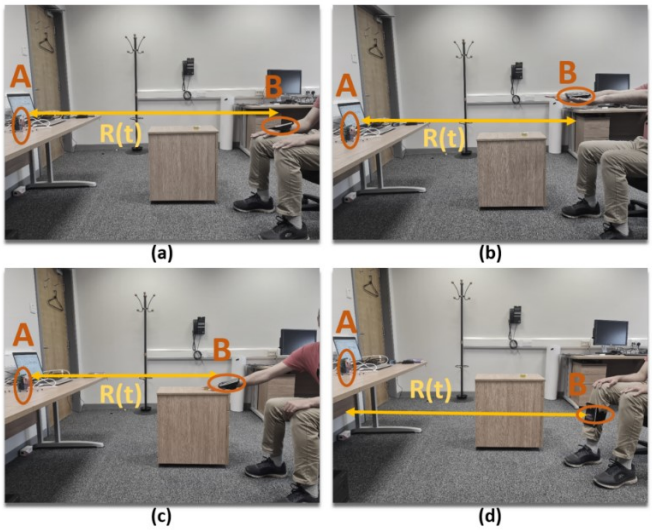

Fig. 7. Data Acquisition for (a) Rest tremor (Upper limb) (b) Postural tremor (c) Action Tremor (d) Rest tremor (Lower limb)

The mobile application gives the three axes raw data for the accelerometer, gyroscope and magnetometer. However, signal processing was performed on the gyroscope and accelerometer readings only. This was done to develop a comparison model as is used in the extant literature. After cleaning and filtering the raw signals, power spectral density analysis was performed to extract frequency while integration was performed on the gyroscope data to calculate amplitude. Algorithms from [21] were adopted for reference amplitude calculation while for reference frequency measurement algorithm described in [46] was implemented. Snapshots of signal processing from both the sensors are given in figures 5 and 6. The data is for a trial of an Action tremor is presented where the frequency calculated for the radar sensor is 6.71 Hz (figure 5e) and the reference sensor is 6.92 Hz (figure 6c). Detailed statistical analysis was performed on the results obtained from both sensors. To evaluate the performance agreement between the proposed methodology and reference sensor, Bland-Altman plots for frequency and amplitude are used [65]. The value of the bias (middle line parallel to the x-axis) in the plots indicates the average value by which the reference method measures more than the proposed one. Corresponding correlation plots are also shown to validate the linear relationship between the predicted value and the reference sensor value for tremor frequency as well as amplitude. The errors for frequency and amplitude values have been calculated for each trial as:

$$F_{error} = f_{predicted} - f_{reference} \quad (14)$$

$$A_{error} = a_{predicted} - a_{reference} \quad (15)$$

A negative value in the error thus indicates that the predicted value by the radar is smaller than the value quantified by the reference sensor. Moreover, the quantified frequency and amplitude have been compared for each tremor type using mean signed error ± standard deviation (ME±SD). The results for each tremor type are first presented separately and then an overall assessment of the proposed method has been carried out. For further analysis, the system performance is also evaluated for dominant and non-dominant limb tremor quantification. Finally, in table X a comparison of the accuracy between our proposed method and the existing non-contact methods is presented. The following sections explain the experimental protocol and the statistical analysis results.

A. Action Tremors

A total of 10 experiments were performed in which the subject was asked to simulate tremor while performing an action as shown in figure 7(c). The subject sat in a chair and acted grabbing an object placed on the table in front of the chair. For the no tremor trials, the subject performed the same action 5 times without simulating tremor. For action tremors, the predicted frequency was found to be in the range of 6 to 10 Hz while the amplitude was calculated to be between 1 and 2 cm. This can be seen in figure 8 which shows the Bland Altman and correlation plots for the 10 trials in which the subject simulated tremor. The bias in frequency is -0.18 Hz, which demonstrates that the overall predicted frequency is slightly lower than the base sensor values. Similarly for the amplitude, the bias is -0.036 cm. Table IV presents the mean signed error for the frequency and amplitude. While performing action tremor trials the data was not collected separately for dominant and non-dominant limbs. This is because the action is always performed using the dominant limb.

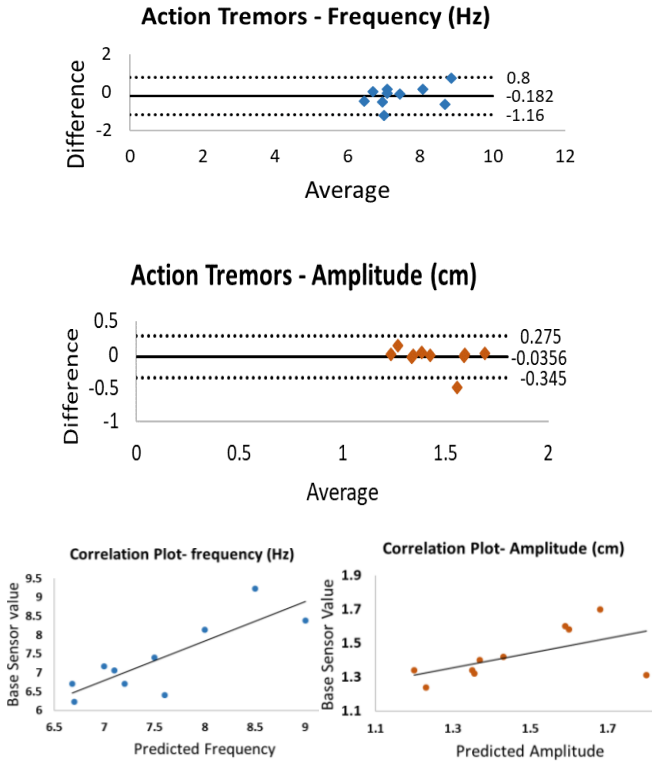

Fig. 8. Bland-Altman and Correlation Plots for Action Tremor

TABLE IV
MEAN ERROR AND STANDARD DEVIATION FOR ACTION TREMOR TRIALS

Tremor Type	*Limb*	*ME ± SD*	
		Frequency (Hz)	*Amplitude (cm)*
Action	Dominant	-0.182 ± 0.50	-0.035 ± 0.16

B. Posture Tremors

For posture tremor, the subject was asked to extend both arms and hold them straight against gravity as shown in figure 7(b). The same was repeated for no tremor trials 5 times, where the subject maintained the extended arm posture without simulating tremor. Figure 9 demonstrates the Bland-Altman and correlation plots for the 10 trials performed for the posture tremors in which the tremor was simulated. It can be seen in figure 9, that the predicted frequency for posture tremor for the trials lies between 6-8 Hz while in two trials it was 9 and 9.8 Hz. The amplitude values are between 1.3 and 2 cm. The mean error values (bias) for frequency and amplitude are -0.15 Hz and -0.115 cm.

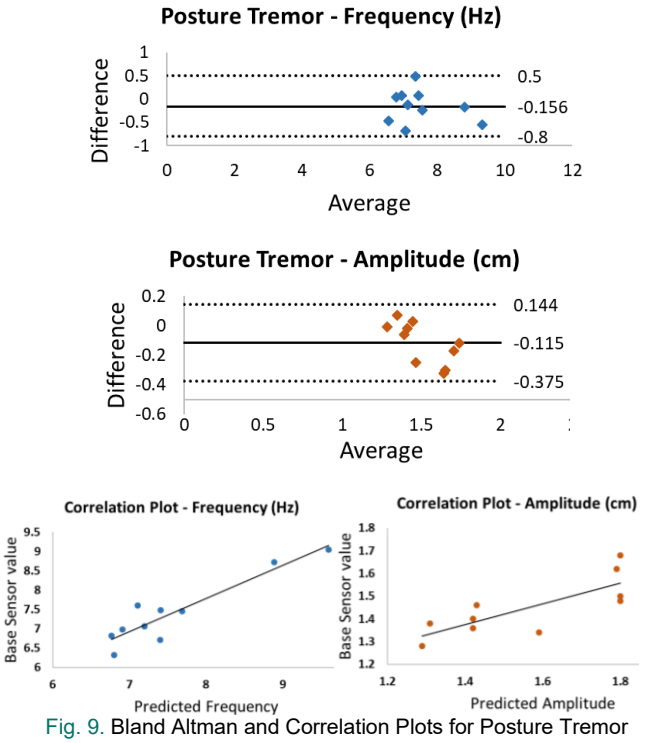

Fig. 9. Bland Altman and Correlation Plots for Posture Tremor

The mean error for the frequency and amplitude of posture tremor trials is given in table V.

TABLE V
MEAN ERROR AND STANDARD DEVIATION FOR POSTURE TREMOR TRIALS

Tremor Type	*Limb*	*ME ± SD*	
		Frequency (Hz)	*Amplitude (cm)*
Posture	Both	-0.156 ± 0.21	-0.115 ± 0.13

C. Rest Tremors (Upper Limb)

To quantify the rest tremors in the upper limbs, the subject sat relaxed in the chair at resting position as shown in figure 7(a). For tremor-induced trials, the subject simulated tremors in the upper limbs while maintaining a sitting position. In the no-tremor trials, the subject kept on sitting relaxed in the chair without simulating tremors. The Bland-Altman plots and the corresponding correlation plots are shown in figure 10. The mean error values for frequency and amplitude are 0.2 Hz and -0.018 cm respectively. The bias in the upper limb tremor frequency is positive indicating that the predicted frequency value is slightly higher than the reference sensor. The predicted frequency values are between 4 and 6 Hz, whereas the amplitude values have been calculated to be between 0.65-1 cm. These ranges are lesser as compared to the action and postural tremor values which shows agreement with the literature as mentioned in table 1.

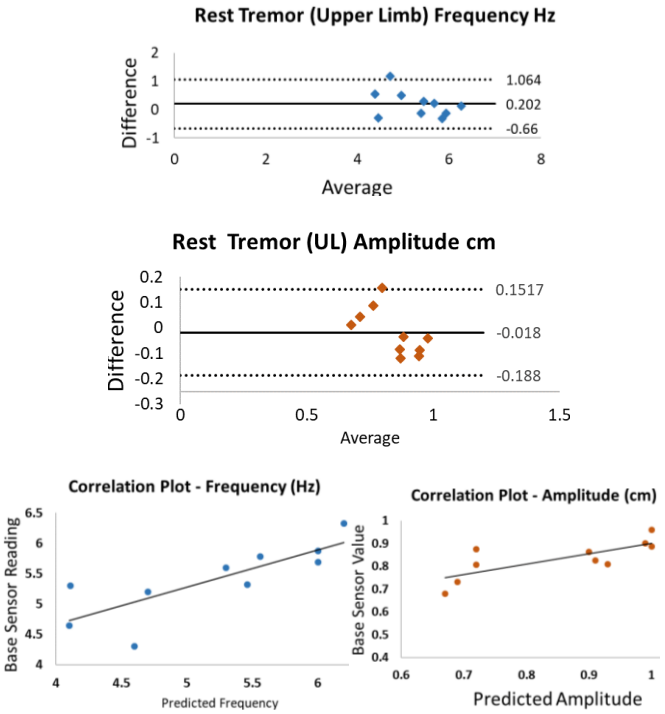

Fig. 10. Bland-Altman and Correlation Plots for Upper limb Rest Tremor

TABLE VI
MEAN ERROR AND STANDARD DEVIATION FOR REST TREMOR IN THE UPPER LIMBS

Tremor Type	*Limb*	*ME ± SD*	
		Frequency (Hz)	*Amplitude (cm)*
Rest Upper Limb	Both	0.202 ± 0.43	-0.018 ± 0.09

D. Rest Tremors (Lower Limb)

For the quantification of rest tremors experienced in the lower limbs, the subject was asked to sit in the chair in a relaxed position. The subject induced tremors in the lower limbs. The mobile is attached to the lower limb as shown in figure 7(d). For the no-tremor trials, the subject sat in a relaxed position in the chair without inducing tremors. Figure 11 illustrates the Bland-Altman and the corresponding correlation graphs for rest lower limb tremors. The frequency and amplitude range for lower limb tremors was found to be between 4 - 6 Hz and 0.6 - 1 cm, respectively. Table VII lists the mean errors for the overall lower rest tremor trials.

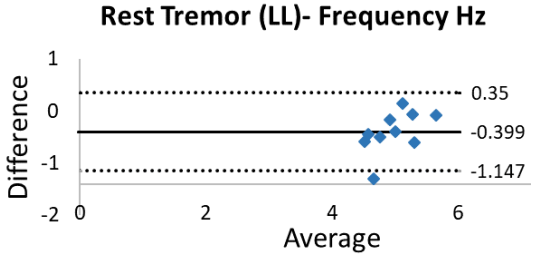

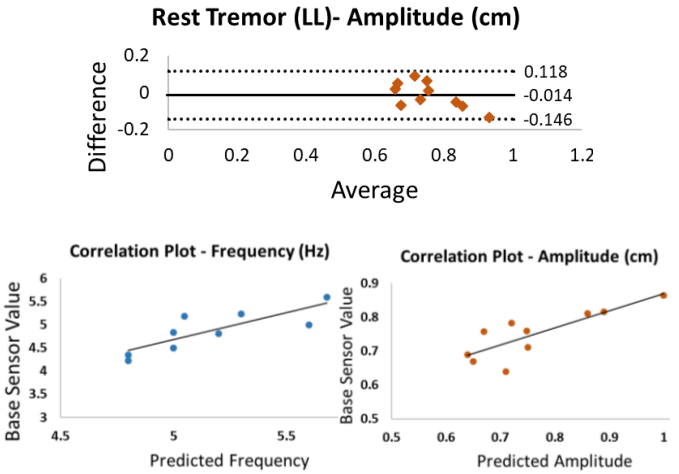

Fig. 11. Bland-Altman and Correlation Plots for Lower limb Rest Tremor

TABLE VII
Mean Error and Standard deviation for Rest tremor in the Lower Limbs

Tremor Type	*Limb*	*ME ± SD*	
		Frequency (Hz)	*Amplitude (cm)*
Rest Lower Limb	Both	-0.399 ± 0.38	-0.014 ± 0.07

E. No Tremor Trials

For each type of tremor, experiments were performed where the subject simulated the action without tremor. The frequency and amplitude in no tremor trials are significantly smaller than those in which the tremor was induced. This is evident from the Bland-Altman and correlation plots as demonstrated in figure 12. It can be observed that the values for frequency and amplitude are 1-2 Hz and 0.2 -0.3 cm respectively. These indicate the slightest body movements or hand movements have given some measurements. This has also been demonstrated through micro-Doppler calculations in the previous work of the authors [44].

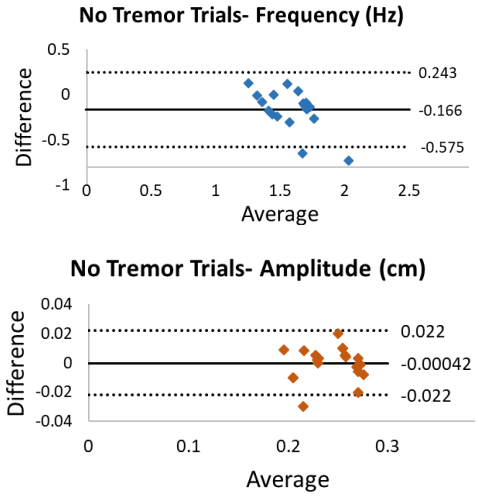

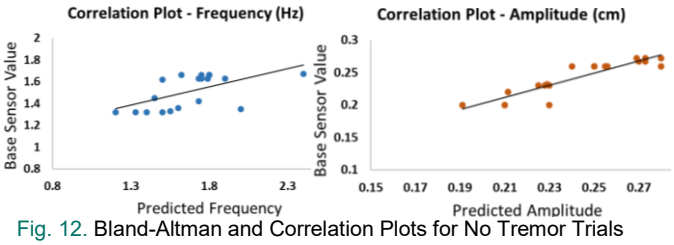

Fig. 12. Bland-Altman and Correlation Plots for No Tremor Trials

TABLE VIII
Mean Error and Standard deviation for No Tremor-Induced Trials

Tremor Type	*ME ± SD*	
	Frequency (Hz)	*Amplitude (cm)*
All trials	-0.166 ± 0.21	-0.0004 ± 0.01
Action	-0.048 ± 0.13	-0.0024 ± 0.01
Posture	-0.098 ± 0.08	0.011 ± 0.004
Upper Limb Rest	-0.146 ± 0.15	-0.006 ± 0.01
Lower Limb Rest	-0.372 ± 0.26	-0.004 ± 0.005

Table VIII presents a summary of the overall mean error and standard deviation for no-tremor trials. It also lists these values for no tremor trials for action, posture, and upper and lower limb tremors.

F. Dominant and Non-Dominant Limbs

To further evaluate the performance of the proposed method, the mean errors for the dominant and non-dominant limbs were calculated separately. Figure 13 visually demonstrates the distribution of normalized errors for the frequency and amplitude values. The errors were normalized for a fair comparison between the dominant and non-dominant sides. From the Interquartile Ranges (IQR) mentioned in the figure 13, it can be observed that mostly the overall spread of the errors is same for both dominant and non-dominant sides. However, the error spread is pronounced for lower limb tremor frequency. Median error bias has also been marked in the box plots. The maximum median bias difference can be observed in the upper limb tremor, with a frequency median bias difference of 0.55 Hz and an amplitude median bias difference of 0.62 cm.

Finally, table IX presents the mean errors for frequency and amplitude for dominant and non-dominant limbs for posture, upper and lower limb tremors. The maximum frequency mean error 0.59 Hz, is observed in the dominant rest lower limb tremor. However, the overall frequency mean errors for dominant and non-dominant sides are smaller than 0.3 Hz. Similarly, the overall amplitude mean errors for dominant and non-dominant sides are smaller than 0.13 cm. This shows that the algorithm can quantify unilateral and bilateral tremors with sensible accuracy.

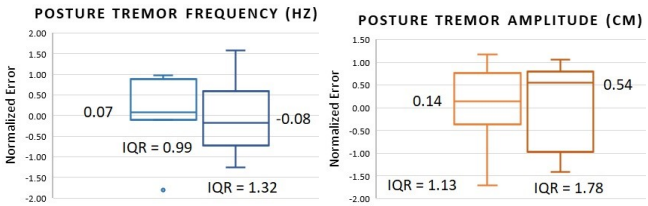

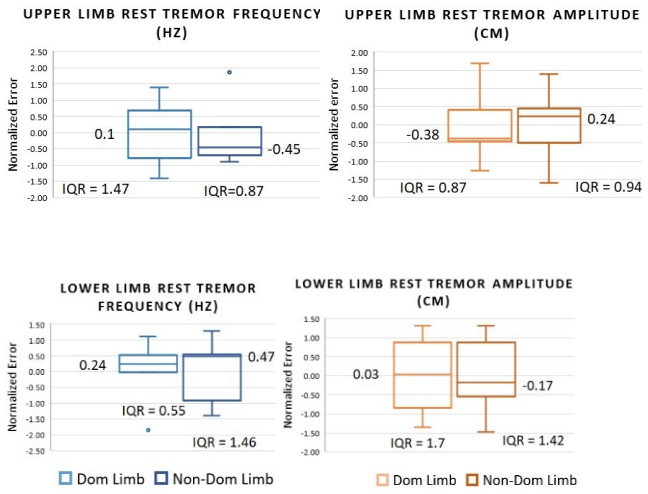

Fig. 13. Box-Plots for Posture, Upper Limb Rest and Lower Limb Rest Tremor for Dominant and Non-Dominant Limbs

TABLE IX
Mean Error and Standard deviation for Dominant and Non-Dominant Limbs

Tremor Type	*Limb*	*ME ± SD*	
		Frequency (Hz)	*Amplitude (cm)*
Posture	Dominant	-0.146 ± 0.22	-0.134 ± 0.09
	Non-Dominant	-0.166 ± 0.42	-0.096 ± 0.15
Rest Upper Limb	Dominant	0.102 ± 0.28	-0.013 ± 0.06
	Non-Dominant	0.302 ± 0.53	-0.023 ± 0.11
Rest Lower Limb	Dominant	-0.592 ± 0.38	0.011 ± 0.06
	Non-Dominant	-0.206 ± 0.27	-0.038 ± 0.07

G. System Performance Summary

The overall mean error (±SD) for the tremor frequency for all 60 experiments was calculated to be -0.144 ± 0.4 Hz while for amplitude it was -0.03 ± 0.1 cm. From tables IV-IX, it can be observed that the mean error calculated by (14) and (15), is mostly negative. The predicted frequency is slightly lower than the reference sensor value 70% of the time (42 trials out of the 60 experiments). Similarly, the predicted tremor amplitude was 55% of the times (33 out of the 60 experiments) marginally less than the reference sensor value. This is evident from tables IV – IX. From these tables, it is also evident that the mean errors in frequency are smaller than 0.4 Hz in all cases except for Upper limb dominant side tremor where the error was 0.59 Hz. For amplitude, the maximum error of 0.13 cm has been observed in the dominant limb Posture tremor. The coefficient of determination was also calculated for both the tremor frequency and amplitude. Overall $R^2 > 0.966$ for both of the parameters and is shown in figures 14 and 15. This indicates a strong correlation between the predicted tremor parameters and the base sensor values.

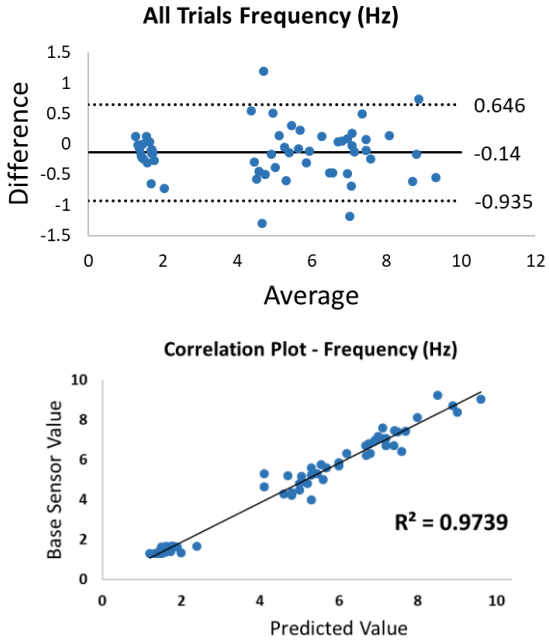

Fig. 14. Bland Altman and Correlation Plots All trials Frequency

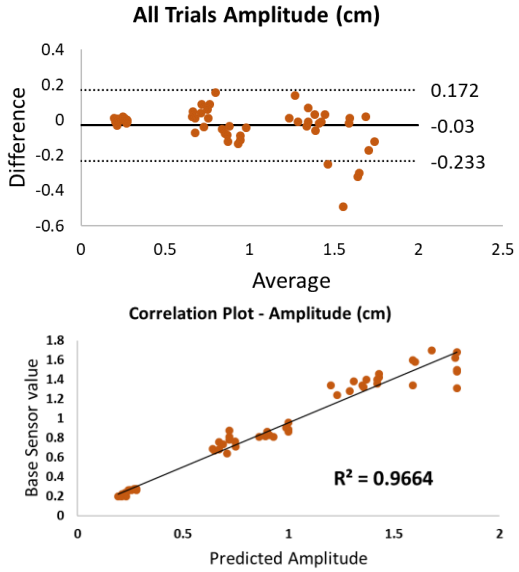

Fig. 15. Bland Altman and Correlation Plots All Trials Amplitude

The box plots in figure 16 give a descriptive statistical summary of the frequency and amplitude errors. The overall spread of the errors for both parameters is significantly small, as evident from their small IQR values also mentioned in the figure.

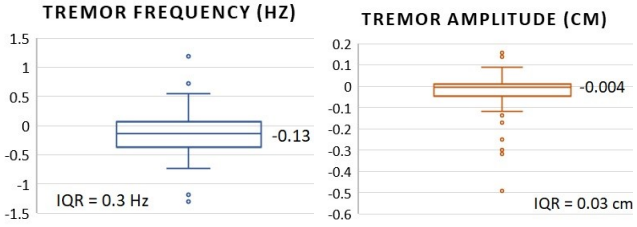

Fig. 16. Box-Plots for Tremor Frequency and Amplitude

H. Comparison with Existing Non-Contact Methods in the Literature

As mentioned in Section II, the non-contact methods that exist in literature are mostly based on cameras. However, this study aimed to develop a methodology which can quantify tremor continuously in a remote setting without invading the privacy of the patient. Hence, a radar sensor was used for the purpose. Table X demonstrates the accuracy comparison between this study and the existing studies that use EM sensors. The studies have also been compared on the type of tremors detected, the maximum range at which the experiments were performed and the tremor parameters quantified. From the table, it is evident that the accuracy achieved by the algorithm developed and the programmed FMCW chirp parameters for the current study is greater than those existing in the literature. Moreover, this study involves extensive experiments performed to quantify various tremors including action, posture and rest tremors. Whereas, existing studies have only quantified hand tremors. The range selected in the current study is comparable to real-home settings. This is also significantly more than those existing in the literature. A summary comparison of this study and existing literature is provided in the table below.

TABLE X
Comparison With Existing Non-Contact Radar Sensor Studies

Study	Range (m)	Tremor Measured	Sensor used	Parameters Quantified	Algorithm Used	Accuracy resolution
This Study	3-6	Action, Posture, Upper Limb Rest & Lower Limb Rest	77 GHz FMCW Radar	Amplitude and Frequency	Vibrational analysis model	0.14 Hz; 0.03 cm $R^2 > 0.966$
[45]	0.2-0.4	Hand Tremor	X Band Doppler radar 2x2 Array	Frequency	Time series data	$R^2 > 0.85$
[41]	1-2	Robotic arm	UWB radar	Amplitude and Frequency	Numerical analysis Linear Minimum Mean Square Error	0.1 cm which decreased as distance increased; 0.01Hz

VI. Conclusion

Tremors deteriorate the ability of a patient to perform everyday simple tasks. The severity of tremors affects the independence and confidence of the patient. Continuous remote monitoring can help in evaluating tremor severity, underlying neurological disease progression and treatment response. This study aimed to develop a system that could unobtrusively quantify tremors while maintaining the integrity and privacy of the patient. For this purpose, the radar was customized to detect tremors and an algorithm was developed to reconstruct tremor trajectories and quantify clinically important parameters pertaining to tremors. The quantified parameters were compared to a reference sensor. Results show a superiority of the proposed methodology with increased accuracy. Moreover, the robustness of the approach is evident from the maximum range at which the tremors can be detected and the comprehensive situations in which tremors are triggered.

References

[1] K. P. Bhatia *et al.*, "Consensus Statement on the classification of tremors. from the task force on tremor of the International Parkinson and Movement Disorder Society," *Mov. Disord.*, vol. 33, no. 1, pp. 75–87, Jan. 2018, doi: 10.1002/MDS.27121.

[2] G. Deuschl *et al.*, "Consensus Statement of the Movement Disorder Society on Tremor," *Mov. Disord.*, vol. 13, no. S3, pp. 2–23, Jan. 1998, doi: 10.1002/MDS.870131303.

[3] G. Zamora, C. Fuchs, A. Degeneffe, P. Kubben, and U. Kaymak, "A smartphone-based clinical decision support system for tremor assessment," *Lect. Notes Comput. Sci. (including Subser. Lect. Notes Artif. Intell. Lect. Notes Bioinformatics)*, vol. 12313 LNBI, pp. 3–12, 2020, doi: 10.1007/978-3-030-63061-4_1/TABLES/4.

[4] A. K. Rao, A. Gilman, and E. D. Louis, "Balance confidence and falls in nondemented essential tremor patients: the role of cognition," *Arch. Phys. Med. Rehabil.*, vol. 95, no. 10, pp. 1832–1837, Oct. 2014, doi: 10.1016/J.APMR.2014.04.001.

[5] "Essential Tremor." https://tremor.org.uk/essential-tremor (accessed Sep. 01, 2022).

[6] "Tremor Fact Sheet | National Institute of Neurological Disorders and Stroke." https://www.ninds.nih.gov/tremor-fact-sheet (accessed Sep. 05, 2022).

[7] "Parkinson disease." https://www.who.int/news-room/fact-sheets/detail/parkinson-disease (accessed Sep. 05, 2022).

[8] S. Bansil *et al.*, "Movement Disorders after Stroke in Adults: A Review," *Tremor and Other Hyperkinetic Movements*, vol. 2, 2012, doi: 10.7916/D86W98TB.

[9] P. Martínez-Martín *et al.*, "Most of the Quality of Life in Essential Tremor Questionnaire (QUEST) psychometric properties resulted in satisfactory values," *J. Clin. Epidemiol.*, vol. 63, no. 7, pp. 767–773, Jul. 2010, doi: 10.1016/j.jclinepi.2009.09.001.

[10] R. J. Elble, "The Essential Tremor Rating Assessment Scale," *J Neurol Neuromedicine*, vol. 1, no. 4, pp. 34–38, 2016, Accessed: Sep. 06, 2022. [Online]. Available: www.jneurology.com

[11] C. G. Goetz, "Movement Disorder Society-Unified Parkinson's Disease Rating Scale (MDS-UPDRS): Une nouvelle échelle pour l'évaluation de la maladie de Parkinson," *Rev. Neurol. (Paris).*, vol. 166, no. 1, pp. 1–4, Jan. 2010, doi: 10.1016/J.NEUROL.2009.09.001.

[12] Y. Liu *et al.*, "Monitoring gait at home with radio waves in Parkinson's disease: A marker of severity, progression, and medication response," *Sci. Transl. Med.*, vol. 14, no. 663, p. eadc9669, Sep. 2022, doi: 10.1126/SCITRANSLMED.ADC9669/SUPPL_FILE/SCITRANSLMED.ADC9669_DATA_FILE_S1.ZIP.

[13] N. Gillani and T. Arslan, "Intelligent Sensing Technologies for the Diagnosis, Monitoring and Therapy of Alzheimer's Disease: A Systematic Review," *Sensors 2021, Vol. 21, Page 4249*, vol. 21, no. 12, p. 4249, Jun. 2021, doi: 10.3390/S21124249.

[14] H. B. Syeda *et al.*, "Amplitude setting and dopamine response of finger tapping and gait are related in Parkinson's disease," *Sci. Reports 2022 121*, vol. 12, no. 1, pp. 1–11, Mar. 2022, doi: 10.1038/s41598-022-07994-8.

[15] A. Salarian, H. Russmann, C. Wider, P. R. Burkhard, F. J. G. Vingerhoets, and K. Aminian, "Quantification of tremor and bradykinesia in Parkinson's disease using a novel ambulatory monitoring system," *IEEE Trans. Biomed. Eng.*, vol. 54, no. 2, pp. 313–322, Feb. 2007, doi: 10.1109/TBME.2006.886670.

[16] Q. Bai *et al.*, "Quantification of the motor symptoms of Parkinson's disease," *Int. IEEE/EMBS Conf. Neural Eng. NER*, pp. 82–85, Aug. 2017, doi: 10.1109/NER.2017.8008297.

[17] R. Powers *et al.*, "Smartwatch inertial sensors continuously monitor real-world motor fluctuations in Parkinson's disease," *Sci. Transl. Med.*, vol. 13, no. 579, Feb. 2021, doi: 10.1126/SCITRANSLMED.ABD7865/SUPPL_FILE/ABD7865_SM.PDF.

[18] J. E. Alty and P. A. Kempster, "A practical guide to the differential diagnosis of tremor," *Postgrad. Med. J.*, vol. 87, no. 1031, pp. 623–629, Sep. 2011, doi: 10.1136/PGMJ.2009.089623.

[19] P. Locatelli, D. Alimonti, G. Traversi, and V. Re, "Classification of Essential Tremor and Parkinson's Tremor Based on a Low-Power Wearable Device," *Electron. 2020, Vol. 9, Page 1695*, vol. 9, no. 10, p. 1695, Oct. 2020, doi: 10.3390/ELECTRONICS9101695.

[20] M. F. Dirkx, H. Zach, B. R. Bloem, M. Hallett, and R. C. Helmich, "The nature of postural tremor in Parkinson disease," *Neurology*, vol. 90, no. 13, pp. e1095–e1103, Mar. 2018, doi: 10.1212/WNL.0000000000005215.

[21] S. Calzetti, M. Baratti, M. Gresty, and L. Findley, "Frequency/amplitude characteristics of postural tremor of the hands in a population of patients with bilateral essential tremor: implications for the classification and mechanism of essential tremor.," *J. Neurol. Neurosurg. Psychiatry*, vol. 50, no. 5, p. 561, 1987, doi: 10.1136/JNNP.50.5.561.

[22] L. A. Sanchez-Perez, L. P. Sanchez-Fernandez, A. Shaout, J. M. Martinez-Hernandez, and M. J. Alvarez-Noriega, "Rest tremor quantification based on fuzzy inference systems and wearable sensors.," *Int. J. Med. Inform.*, vol. 114, pp. 6–17, Mar. 2018, doi: 10.1016/J.IJMEDINF.2018.03.002.

[23] M. J. Johnson, "Detection of Parkinson Disease Rest Tremor," *McKelvey Sch. Eng. Theses Diss.*, Aug. 2014, doi: https://doi.org/10.7936/K7W66HQ8.

[24] L. Fraiwan, R. Khnouf, and A. R. Mashagbeh, "Parkinson's disease hand tremor detection system for mobile application," *http://dx.doi.org/10.3109/03091902.2016.1148792*, vol. 40, no. 3, pp. 127–134, Apr. 2016, doi: 10.3109/03091902.2016.1148792.

[25] M. Moazami-Goudarzi, J. Sarnthein, L. Michels, R. Moukhtieva, and D. Jeanmonod, "Enhanced frontal low and high frequency power and synchronization in the resting EEG of parkinsonian patients," *Neuroimage*, vol. 41, no. 3, pp. 985–997, Jul. 2008, doi: 10.1016/J.NEUROIMAGE.2008.03.032.

[26] C. Ma *et al.*, "Quantitative assessment of essential tremor based on machine learning methods using wearable device," *Biomed. Signal Process. Control*, vol. 71, p. 103244, Jan. 2022, doi: 10.1016/J.BSPC.2021.103244.

[27] S. M. Ali *et al.*, "Wearable sensors during drawing tasks to measure the severity of essential tremor," *Sci. Reports 2022 121*, vol. 12, no. 1, pp. 1–10, Mar. 2022, doi: 10.1038/s41598-022-08922-6.

[28] H. Dai, P. Zhang, and T. C. Lueth, "Quantitative Assessment of Parkinsonian Tremor Based on an Inertial Measurement Unit," *Sensors (Basel).*, vol. 15, no. 10, p. 25055, 2015, doi: 10.3390/S151025055.

[29] D. Y. Kwon, Y. R. Kwon, Y. H. Choi, G. M. Eom, J. Ko, and J. W. Kim, "Quantitative measures of postural tremor at the upper limb joints in patients with essential tremor," *Technol. Heal. Care*, vol. 28, no. S1, pp. 499–507, Jan. 2020, doi: 10.3233/THC-209050.

[30] F. Lipsmeier *et al.*, "Reliability and validity of the Roche PD Mobile Application for remote monitoring of early Parkinson's disease," *Sci. Reports 2022 121*, vol. 12, no. 1, pp. 1–15, Jul. 2022, doi: 10.1038/s41598-022-15874-4.

[31] N. Akram *et al.*, "Developing and assessing a new web-based tapping test for measuring distal movement in Parkinson's disease: a Distal Finger Tapping test," *Sci. Rep.*, vol. 12, no. 1, Dec. 2022, doi: 10.1038/S41598-021-03563-7.

[32] P. L. Kubben, M. L. Kuijf, L. P. C. M. Ackermans, A. F. G. Leentjes, and Y. Temel, "TREMOR12: An Open-Source Mobile App for Tremor Quantification.," *Stereotact. Funct. Neurosurg.*, vol. 94, no. 3, pp. 182–186, Jul. 2016, doi: 10.1159/000446610.

[33] R. López-Blanco *et al.*, "Essential tremor quantification based on the combined use of a smartphone and a smartwatch: The NetMD study," *J. Neurosci. Methods*, vol. 303, pp. 95–102, Jun. 2018, doi: 10.1016/J.JNEUMETH.2018.02.015.

[34] P. Mcgurrin, J. Mcnames, T. Wu, M. Hallett, and D. Haubenberger, "Quantifying Tremor in Essential Tremor Using Inertial Sensors—Validation of an Algorithm," *IEEE J. Transl. Eng. Heal. Med.*, vol. 9, 2021, doi: 10.1109/JTEHM.2020.3032924.

[35] J. Kim, T. Wichmann, O. T. Inan, and S. P. Deweerth, "Fitts' Law Based Performance Metrics to Quantify Tremor in Individuals With Essential Tremor," *IEEE J. Biomed. Heal. Informatics*, vol. 26, no. 5, pp. 2169–2179, May 2022, doi: 10.1109/JBHI.2021.3129989.

[36] A. Garcia-Agundez and C. Eickhoff, "Towards Objective Quantification of Hand Tremors and Bradykinesia Using Contactless Sensors: A Systematic Review," *Front. Aging Neurosci.*, vol. 13, p. 694, Oct. 2021, doi: 10.3389/FNAGI.2021.716102/XML/NLM.

[37] M. A. Alper, J. Goudreau, and M. Daniel, "Pose and Optical Flow Fusion (POFF) for accurate tremor detection and quantification," *Biocybern. Biomed. Eng.*, vol. 40, no. 1, pp. 468–481, Jan. 2020, doi: 10.1016/J.BBE.2020.01.009.

[38] S. Sooklal, P. Mohan, and S. Teelucksingh, "Using the Kinect for detecting tremors: Challenges and opportunities," *2014 IEEE-EMBS Int. Conf. Biomed. Heal. Informatics, BHI 2014*, pp. 768–771, 2014, doi: 10.1109/BHI.2014.6864477.

[39] F. Fioranelli, J. Le Kernec, and S. A. Shah, "Radar for Health Care: Recognizing Human Activities and Monitoring Vital Signs," *IEEE Potentials*, vol. 38, no. 4, pp. 16–23, Jul. 2019, doi: 10.1109/MPOT.2019.2906977.

[40] C. Li, V. M. Lubecke, O. Boric-Lubecke, and J. Lin, "A review on recent advances in doppler radar sensors for noncontact healthcare monitoring," *IEEE Trans. Microw. Theory Tech.*, vol. 61, no. 5, pp. 2046–2060, 2013, doi: 10.1109/TMTT.2013.2256924.

[41] G. Blumrosen, M. Uziel, B. Rubinsky, and D. Porrat, "Non-contact UWB radar technology to assess tremor," *IFMBE Proc.*, vol. 29, pp. 490–493, 2010, doi: 10.1007/978-3-642-13039-7_123/COVER.

[42] C. I. Radar, A. Manager, and S. Rao, "The fundamentals of millimeter wave radar sensors The fundamentals of millimeter wave radar sensors 2," 2020.

[43] X. Yang *et al.*, "S-Band Sensing-Based Motion Assessment Framework for Cerebellar Dysfunction Patients," *IEEE Sens. J.*, vol. 19, no. 19, pp. 8460–8467, Oct. 2019, doi: 10.1109/JSEN.2018.2861906.

[44] N. Gillani and T. Arslan, "Unobtrusive Detection and Monitoring of Tremors using Non-Contact Radar Sensor," *BioSMART 2021 - Proc. 4th Int. Conf. Bio-Engineering Smart Technol.*, 2021, doi: 10.1109/BIOSMART54244.2021.9677856.

[45] C. H. Lin, J. X. Wu, J. C. Hsu, P. Y. Chen, N. S. Pai, and H. Y. Lai, "Tremor Class Scaling for Parkinson Disease Patients Using an Array X-Band Microwave Doppler-Based Upper Limb Movement Quantizer," *IEEE Sens. J.*, vol. 21, no. 19, pp. 21473–21485, Oct. 2021, doi: 10.1109/JSEN.2021.3103803.

[46] P. L. Kubben, M. L. Kuijf, L. P. C. M. Ackermans, A. F. G. Leentjes, and Y. Temel, "TREMOR12: An Open-Source Mobile App for Tremor Quantification," *Stereotact. Funct. Neurosurg.*, vol. 94, no. 3, pp. 182–186, Aug. 2016, doi: 10.1159/000446610.

[47] G. Zamora, C. Fuchs, A. Degeneffe, P. Kubben, and U. Kaymak, "A smartphone-based clinical decision support system for tremor assessment," *Lect. Notes Comput. Sci. (including Subser. Lect. Notes Artif. Intell. Lect. Notes Bioinformatics)*, vol. 12313 LNBI, pp. 3–12, 2020, doi: 10.1007/978-3-030-63061-4_1/TABLES/4.

[48] Y.-J. Zhong and Q.-S. Li, "Human Motion Recognition in Small Sample Scenarios Based on GaN and CNN Models," *Prog. Electromagn. Res. M*, vol. 113, pp. 101–113, 2022, doi: 10.2528/PIERM22070204.

[49] N. Kern, J. Aguilar, T. Grebner, B. Meinecke, and C. Waldschmidt, "Learning on Multistatic Simulation Data for Radar-Based Automotive Gesture Recognition," *IEEE Trans. Microw. Theory Tech.*, pp. 1–12, 2022, doi: 10.1109/TMTT.2022.3200595.

[50] D. G. Bresnahan and Y. Li, "Classification of Driver Head Motions Using a mm-Wave FMCW Radar and Deep Convolutional Neural Network," *IEEE Access*, vol. 9, pp. 100472–100479, 2021, doi: 10.1109/ACCESS.2021.3096465.

[51] M. A. Richards, J. A. Scheer, and W. A. Holm, "Principles of modern radar: Basic principles," *Princ. Mod. Radar Basic Princ.*, pp. 1–925, Jan. 2010, doi: 10.1049/sbra021e.

[52] V. C. Chen, "The Micro-Doppler Effect in Radar, Second Edition,"

J. Chem. Inf. Model., pp. 115–123, 2019.
[53] "AWR1642BOOST Evaluation board | TI.com." https://www.ti.com/tool/AWR1642BOOST (accessed Oct. 09, 2022).
[54] S. Rao and J. C. Roh, "77GHz single chip radar sensor enables automotive body and chassis applications Adeel Ahmad".
[55] "DCA1000EVM Evaluation board | TI.com." https://www.ti.com/tool/DCA1000EVM?login-check=true (accessed Oct. 09, 2022).
[56] "MMWAVE-STUDIO IDE, configuration, compiler or debugger | TI.com." https://www.ti.com/tool/MMWAVE-STUDIO (accessed Oct. 09, 2022).
[57] K. Ramasubramanian, "Using a complex-baseband architecture in FMCW radar systems," 2017.
[58] W. Carrara, R. Goodman, and R. Majewski, "Spotlight synthetic aperture radar : signal processing algorithms," *undefined*, 1995.
[59] J. Muñoz-Ferraras, F. Pérez-Martínez, and M. Burgos-García, "Helicopter classification with a high resolution LFMCW radar," *IEEE Trans. Aerosp. Electron. Syst.*, vol. 45, no. 4, p. 1373, Oct. 2009, doi: 10.1109/TAES.2009.5310305.
[60] "US20160054438A1 - Vibration parameters monitoring using fmcw radar - Google Patents." https://patents.google.com/patent/US20160054438A1/en (accessed Sep. 17, 2022).
[61] M. Alizadeh, G. Shaker, J. C. M. De Almeida, P. P. Morita, and S. Safavi-Naeini, "Remote monitoring of human vital signs using mm-Wave FMCW Radar," *IEEE Access*, vol. 7, pp. 54958–54968, 2019, doi: 10.1109/ACCESS.2019.2912956.
[62] T. K. V. Dai *et al.*, "Enhancement of Remote Vital Sign Monitoring Detection Accuracy Using Multiple-Input Multiple-Output 77 GHz FMCW Radar," *IEEE J. Electromagn. RF Microwaves Med. Biol.*, vol. 6, no. 1, pp. 111–122, Mar. 2022, doi: 10.1109/JERM.2021.3082807.
[63] P. CRAWFORD and E. E. ZIMMERMAN, "Differentiation and Diagnosis of Tremor," *Am. Fam. Physician*, vol. 83, no. 6, pp. 697–702, Mar. 2011, Accessed: Sep. 05, 2022. [Online]. Available: https://www.aafp.org/pubs/afp/issues/2011/0315/p697.html
[64] "Assessment of tremor - Differential diagnosis of symptoms | BMJ Best Practice." https://bestpractice.bmj.com/topics/en-gb/974?locale=ko (accessed Sep. 05, 2022).
[65] D. Giavarina, "Understanding Bland Altman analysis," *Biochem. Medica*, vol. 25, no. 2, p. 141, 2015, doi: 10.11613/BM.2015.015.

NAZIA GILLANI did her B.Sc. in Electrical Engineering in telecommunication from the University of Engineering and Technology Lahore, Pakistan. She earned her M.Sc. in Electrical Engineering with a specialization in Electronics and Embedded Systems from the Lahore University of Management Sciences in 2012. Currently, she is pursuing her PhD at the School of Engineering, The University of Edinburgh, Edinburgh, U.K. Her research focuses on unobtrusive sensing of movement disorders through RF and microwave sensors. She has worked as a System Design Engineer in Global Engineering Services, Pakistan, which is an offshore office for Whizz Systems, Silicon Valley, USA. She also has more than 5 years of experience as a faculty member in the Electrical Engineering department of the University of Central Punjab, Pakistan.

TUGHRUL ARSLAN holds the Chair of Integrated Electronic Systems with the School of Engineering, The University of Edinburgh, Edinburgh, U.K. He is a member of the Integrated Micro and Nano Systems (IMNS) Institute and leads the Embedded Mobile and Wireless Sensor Systems (EWireless) Group with the University (ewireless.eng.ed.ac.UK). His research interests include developing low-power radio frequency sensors for wearable and portable biomedical applications. He is the author of more than 500 refereed papers and the inventor of more than 20 patents. He is currently an Associate Editor of the IEEE Transactions on Very Large Scale Integration (VLSI) systems and was previously an Associate Editor of the IEEE Transactions on Circuits and Systems-I: Regular papers (2005-2006) and IEEE Transactions on Circuits and Systems-II: Express briefs (2008-2009). He is also a member of the IEEE CAS Executive Committee on VLSI Systems and Applications, in 1999, and a member of the steering and technical committees of several international conferences. He is a Co-Founder of the NASA/ESA Conference on Adaptive Hardware and currently serves as a member of its steering committee.

GILLIAN MEAD is Professor of Stroke and Elderly Care Medicine at the Usher Institute in the University of Edinburgh. Her research aims to find out how to improve recovery and quality of life of people who survive a stroke and is driven by the clinical needs of patients. She employs a variety of research designs, including systematic reviews, observational studies, qualitative research methodology and randomised controlled clinical trials. Professor Mead's research is focused on the under-researched area of 'Life after Stroke'. She leads programmes of research in fatigue, exercise and cognition after stroke; these topics are amongst the top 10 priorities for stroke research. She is a co-principal investigator of the FOCUS Trial (Fluoxetine or control Under Supervision), a UK multicentre trial that seeks to determine whether fluoxetine improves recovery after stroke. In addition, Professor Mead also works in the Advanced Care Research Centre.